Control Optimization for a Power-Split Hybrid Vehicle

Jinming Liu Huei Peng

Abstract— **Toyota Hybrid System (THS) is used in the current best-selling hybrid vehicle on the market—the Toyota Prius. This hybrid system contains a power split planetary gear system which combines the benefits of series and parallel hybrid vehicles. This paper first develops a dynamic model to investigate the control strategy of the THS power train. An Equivalent Consumption Minimization Strategy (ECMS) is developed which is based on instantaneous optimization concept. The Dynamic Programming (DP) technique is then utilized to obtain a performance benchmark and insight toward fine-tuning of the ECMS algorithm for better performance.**

I. Introduction

THE pursue of fuel efficiency for ground vehicles has accelerated in recently years due to escalated fossil fuel price and increased environmental concerns. Conventional ground vehicle power train uses an internal combustion engine as the only power source. A hybrid electric vehicle (HEV) adds an electric power path to the conventional mechanical power path. This additional input helps to improve fuel economy mainly by engine down-sizing/right-sizing, load leveling, and re-generative braking.

The HEV power train can be divided into three categories based on their configurations: parallel hybrids, series hybrids, and power split hybrids. The parallel configuration, as shown in Fig. 1A, includes two separate power paths. The engine transmission path and battery motor path can drive the vehicle individually or simultaneously [1]. However, since the motor can not charge the battery and assist the engine at the same time, the power storage only lasts for a short time and the power assistance has to be constrained to avoid the drain of the battery. The series configuration, as shown in Fig. 1B, only applies motor (sometimes motors) to drive the wheels. The motor power is supplied by either a battery, or a generator transforming the mechanical power from the engine into electrical power, or the combination of both. Since the engine operation is independent of the vehicle speed and road condition, it is controlled to operate near its optimal condition for most of the time. A disadvantage of such configuration, however, is that the efficiency of the electric machine(s) will reduce the overall performance since the engine can not directly supply the power [2].

The power train configuration of the power split hybrid system, sometimes referred as parallel/series hybrid, combines the previous two configurations with a power split device, as shown in Fig. 1C. It is appealing because with proper control strategy it can be designed to take advantage of both parallel and series types and avoid their disadvantages.

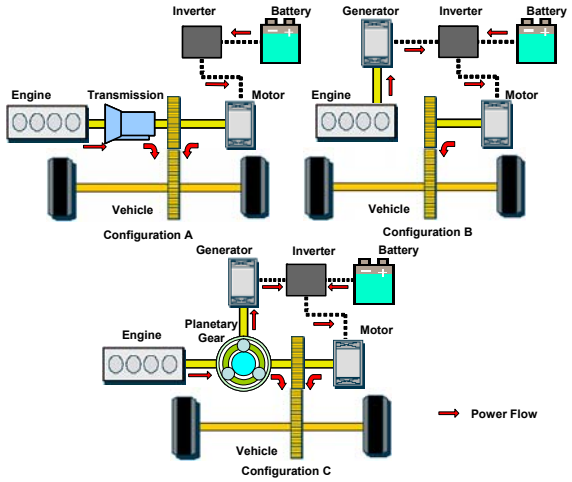

Fig. 1. Hybrid vehicle configurations: A. Parallel; B. Series; C. Power Split (parallel/series).

Studies on power split mechanisms can be traced back to the 70s by a work by Gelb et al. [3]. Earlier version of such devices appeared in the hydrostatic power split transmission commonly used on lawn tractors. Miller et al. [4] provided a historical perspective of the power split device development. THS, the core of the first commercial power-split HEV offered on the market, was described in details by Sasaki [5] in Japan in 1998, and Harada et al. [6]. Hermance [7] presented it to the US in year 1999 and Kimura, et al. [8] explained the force control strategy. The early models of Toyota Prius were tested by the Argonne National Lab [9]. The experiment data was used for the according developed vehicle models in PSAT [10] and ADVISOR [11]. Through this process, Duoba et al. [12] provided in-depth characterization and experimental comparison of Toyota Prius and Honda Insight. In year 2004, Toyota released an improved THS system (THS II). Muta, et al. [13] and Kawahashi [14] offered comparison study between the old and new THS power split systems. Such configuration is implemented in SUV in 2005 and the development is described by Akihiro et al. [15]. Other related efforts in this area includes: a split-type hybrid vehicle model was developed and optimal control algorithm studied in [16] by using the dynamic programming technique. This model does not analyze detail component behavior. Rizoulis et al. [17] presented a mathematical model of a vehicle with a power split device based on the steady state transmission

The authors are with the Department of Mechanical Engineering, University of Michigan, Ann Arbor, MI, 48109-2133 USA. (Contact: hpeng@umich.edu, 1-734-936-0352).

performance. Despite of these efforts, few of the past publications offered a clear explanation of the control algorithm of THS, or in general, for power-split hybrid systems. Since control algorithms are becoming the core of modern hybrid vehicles,

A dynamic model is presented in this paper. It can be applied to both THS and THSII by varying the component parameters, because the power split gear set remains the same for both—i.e., the basic dynamic equations governing the vehicle remain unchanged [13]. The enhancement from the first generation to second generation of THS includes improved component sizing, higher efficiency, and increased electric machine operating range.

Equivalent consumption minimization strategy (ECMS) is applied to generate an optimal power management control strategy. This algorithm is derived by Paganelli et al. [18] and is based on instantaneous optimization concept. The dynamic programming (DP) technique is a horizon based optimization concept and can be used to fully explore the potential of the power split power train [1, 19]. Due to its preview nature and heavy computational requirements, it is not implementable and is used only to obtain a benchmark for improving other control strategies. In this paper, the DP solution is used to improve the ECMS control strategy—which is not optimal in any sense, but it demonstrates the usage of the DP results quite well.

II. Modeling of Toyota Hybrid System (THS)

THS uses a planetary gear as the power split device [7]. It consists of a ring gear, a sun gear, a carrier gear and several pinion gears. As a result of the mechanical connection through gear teeth, the rotational speeds of the ring gear ω_r, sun gear ω_s, and the carrier gear ω_c satisfy the following relationship

$$\omega_s S + \omega_r R = \omega_c (R + S) \tag{1}$$

where R, and S are the radii of the ring gear and sun gear respectively. A lever diagram introduced by Benford [20] is commonly used to present the speed constraint which simplifies the torque analysis for the planetary gear set, as shown in Fig. 2.

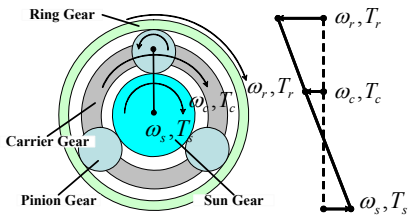

Fig. 2. Lever diagram to present the planetary gear set.

Fig. 3 shows the free body diagram of the THS power train without the electrical sub-systems. The sun gear, the carrier gear, and the ring gear are connected to one of the motor/generator, M/G 1, engine and vehicle, respectively. In addition, another electric motor/generator, M/G 2 is also attached to the ring gear, which enables direct motor propulsion and efficient regenerative braking. The power generated by the engine is split into two paths: a mechanical path and an electrical path. The mechanical path consists of power transferred from the carrier gear directly to the ring gear, which is connected to the final drive of the vehicle. The electrical path takes the rest of the engine power, transforms it into the electrical form through the M/G 1. The power is then either pumped into the battery, or supplied to the M/G 2.

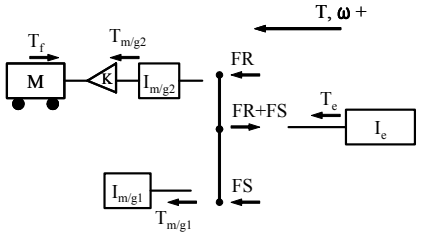

Fig. 3. Free body diagram of the mechanical path of THS.

The detail dynamic equations were described in [21] and will be summarized below. If we analyze the dynamic of each node by assuming zero pinion gear inertia and vehicle longitudinal dynamics only, three equations will be generated as follows

$$\dot{\omega}_{m/g1}(I_{m/g1} + I_s) = F \cdot S - T_{m/g1} \tag{2}$$

$$\dot{\omega}_e(I_e + I_c) = T_e - F \cdot R - F \cdot S \tag{3}$$

$$\dot{\omega}_r\left(\frac{R_{tire}^2}{K} m + I_{m/g2} K + I_r K\right) = (T_{m/g2} + F \cdot R)K - T_f - mgf_r R_{tire} - 0.5\rho A C_d \left(\frac{\omega_r}{K}\right)^2 R_{tire}^{\ 3} \tag{4}$$

where $T_{m/g1}$, $T_{m/g2}$, and T_e are the input torques to the ring gear shaft, the sun gear shaft, and the carrier shaft respectively, I_r, I_s, and I_c are the corresponding inertia. $I_{m/g1}$, $I_{m/g2}$, and I_e, are the power source inertia. F presents the internal force on the pinion gears, m is the vehicle weight. T_f is the brake torque applied by the traditional friction brake system. K is the final drive ratio, R_{tire} is the tire radius, f_r is the rolling resistance coefficient, and $0.5\rho AC_d$ presents the aerodynamic drag resistance coefficient. To simplify the equations, we assume there is no viscous or Coulomb frictions. Equations (1)-(4) can be presented in a matrix form as follows

$$\begin{bmatrix} I_s + I_{m/g1} & 0 & 0 & -S \\ 0 & I_c + I_e & 0 & R + S \\ 0 & 0 & \frac{R_{tire}^2}{K} m + I_{m/g2} K + I_r K & -KR \\ S & -(R+S) & R & 0 \end{bmatrix} \begin{bmatrix} \dot{\omega}_{m/g1} \\ \dot{\omega}_e \\ \dot{\omega}_r \\ F \end{bmatrix} = \begin{bmatrix} T_{m/g1} \\ T_e \\ KT_{m/g2} - T_{fb} - mgf_r R_{tire} - 0.5\rho A C_d \left(\frac{\omega_r}{K}\right)^2 R_{tire}^{\ 3} \\ 0 \end{bmatrix} \tag{5}$$

Although there are four equations, one of them shows the speed relation and one tracks the internal force F which can be eliminated through further simplification. Therefore, the actual number of degree of freedom is two.

To completely describe the status of the vehicle, one more state variable needs to be defined for the battery State of

Charge. It depends on the equivalent battery capacity C_{batt} and the current flowing through I_{batt} :

$$\dot{SOC} = -\frac{I_{batt}}{C_{batt}} \tag{6}$$

where I_{batt} is the battery current and C_{batt} is the battery capacity. An internal resistance model is used, from which the battery power output is

$$P_{batt} = V_{oc} I_{batt} - I_{batt}^2 R_{batt} \tag{7}$$

where V_{oc} is the open circuit voltage and R_{batt} is the battery resistance, both are functions of SOC. Note here when P_{batt} and I_{batt} are both positive, the battery is discharging. When they are negative, the battery is charging.

Equation (7) shows the relationship between battery current and power. However, in the simulations, we specify the motor/generator power instead of battery current, and the battery power is calculated from

$$P_{batt} = T_{m/g1}\omega_{m/g1}\eta_{m/g1}^{\ k} + T_{m/g2}\omega_{m/g2}\eta_{m/g2}^{\ k} \tag{8}$$

where $\eta_{m/g1}$ and $\eta_{m/g2}$ are the efficiency of the motor/generators. $k=-1$ when the battery is discharged and $k=1$ when the battery is charged. Based on (6)-(8), we have

$$\dot{SOC} = \frac{V_{oc} - \sqrt{V_{oc}^{\ 2} - 4(T_{m/g1}\omega_{m/g1}\eta_{m/g1}^{\ k} + T_{m/g2}\omega_{m/g2}\eta_{m/g2}^{\ k})R_{batt}}}{C_{batt}} \tag{9}$$

which is the governing equation of the battery dynamics. Plus the mechanical dynamics of (5), it completes the dynamic model for THS. All the vehicle parameters, engine maps and efficiency look-up tables of the simulation are obtained from ADVISOR 2002 [11] and they are for the THS (2001-2003 Prius in the US).

III. Control of THS

The two electrical power sources in a split hybrid vehicle can be viewed as a "speeder" and a "torquer". The "speeder" is controlled to manipulate the speed of the engine and the "torquer" helps to balance the torque requirement. In the THS, the smaller M/G 1 is utilized to control the engine speed and the bigger M/G 2 assists the engine with additional torque [7].

Such divide-and-conquer architecture decouples the multiple-input control design into two steps of system optimization and engine optimization (See Fig. 4). The overall power demand for the vehicle can be supplied by engine and by battery, individually or simultaneously. This is achieved by a higher level power management controller. After the engine power demand is specified, a predefined optimal engine speed for such power demand can be computed. And this desired speed is achieved by manipulating the electric machine, M/G 1. The rest of the power demand is supplied by the other electric machine, M/G 2. This procedure is called engine optimization. M/G 2 is also used for regenerative breaking.

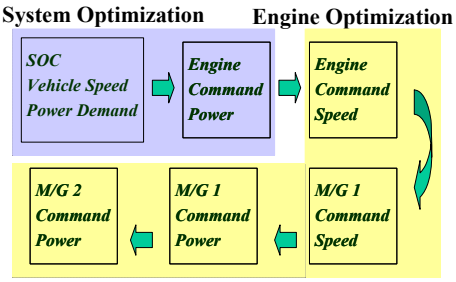

Fig. 4. Decoupled control of the THS power train.

The control for engine optimization can be found in many references, [6, 8, 12]. It determines best engine efficiency based on engine power demand. However, the engine power selection also affects the overall system efficiency and fuel economy. Hermance [7] presented a rule based approach which is said to the basic concept of the control algorithm implemented in the Prius. Our earlier study implemented such design which demonstrated vehicle behavior similar to test results [21]. Although this simple control offers a working solution quickly, it does not offer any idea of the level of optimality.

The Equivalent consumption minimization strategy (ECMS) [18] is based on the concept of instantaneous equivalent fuel consumption. It is calculated by defining an equivalent total fuel consumption as

$$\dot{m}_{f\_equi}(t) = \dot{m}_{f\_eng} + f(soc)\cdot\dot{m}_{f\_batt} \tag{10}$$

where

$$\dot{m}_{f\_batt} = \frac{SC_{eng}\cdot P_{batt}}{Eff_{m/g}} \tag{11}$$

In (11), $\dot{m}_{f\_batt}$ represents the equivalent fuel consumption of the electric power. The average engine fuel consumption SC_{eng} is selected based on the engine fuel map. Similarly, the average power efficiency of the motor/generator $Eff_{m/g}$ is selected from its efficiency map. This results in an approximated equivalent fuel consumption value regardless of the speed and torque of the engine and the motor/generator. Therefore, Equation (11) is only an approximation. $f(soc)$ is a weighting factor (See Fig. 5) to achieve SOC regulation. It sets the target SOC at around 0.6 and weights the SOC away from this target value by varying the additional weight $f(soc)$.

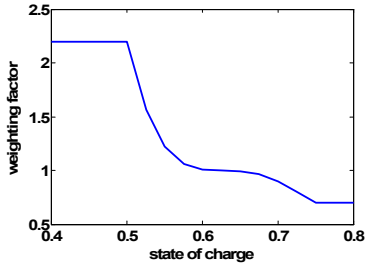

Fig. 5. SOC weighting factor $f(SOC)$ for the ECMS algorithm.

Given a driver power demand, the optimal engine power can be calculated by comparing all the possible solutions and select the engine power that achieves minimal

equivalent fuel consumption. The calculated optimal engine power map is determined offline and is as shown in Fig. 6. This map is implemented as part of the power management controller.

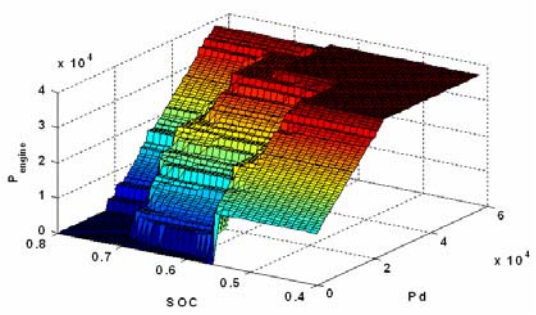

Fig. 6. Optimized ECMS engine power map.

IV. Dynamic Programming for THS

Dynamic programming (DP) [19] is a multi-stage decision-making process involving a dynamic system, a cost function and a state grid. It is a tool to solve general dynamic optimization problems. The optimal control signal is generated backwards along a horizon according to a predefined cost function. This cost function is optimized within the boundary of the state grid. This algorithm guarantees global optimal solution up to the grid accuracy of the states for both linear and nonlinear systems. Furthermore, it is flexible in accommodating different definitions of cost functions or state and input constraints. However, a major limitation of the dynamic programming is the extreme computational load. As the number of state variables increases the computation time and the memory storage increase exponentially. Therefore, several techniques are applied to reduce the computation cost and speed up the computation time.

Fig. 7 shows the formulation of the single-step transition model for the THS optimization. There are three states, two inputs and one disturbance signal. The three states are engine speed ω_e, ring gear speed ω_r, and battery SOC. The system actually has three control inputs from M/G 1 (T_g), engine (*Throttle*), and M/G 2 (T_m). However, since the demand power P_d is supplied by

$$P_d = P_e + P_{m/g1} + P_{m/g2} \tag{12}$$

where P_e, $P_{m/g1}$, and $P_{m/g2}$ are the power from the engine and the two motor generators. If the vehicle is controlled to follow a predefined driving cycle, one of the control, which we select to be $T_{m/g2}$ in this paper, is no longer free and can be calculated from

$$T_{m/g2} = (P_d - T_e \cdot \omega_e - T_{m/g1} \cdot \omega_{m/g1}) / \omega_{m/g2} \tag{13}$$

where T_e and $\omega_{m/g2}$ are both calculated from the states and input signals. The selected grid points are shown in Table I. The grid sizes of the state are important because they are directly related to the simulation accuracy and computation time. Small grid sizes lead to longer computation time but more accurate optimization results.

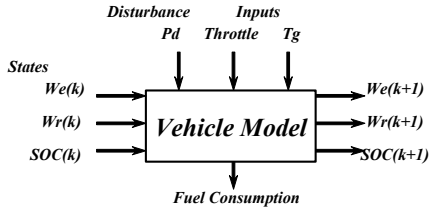

Fig. 7. Single-step transition model of the THS.

TABLE I
SELECTED GRIDS FOR DP PROBLEM OF THS

	Variables	Grids
States	Engine Speed (rpm)	1000:100:4000
	Ring Gear Speed (rpm)	Specified by driving cycle
	State of Charge	0.4:0.003:0.7
Inputs	Engine Throttle (0~1)	0:0.025:1
	M/G 1 Torque (Nm)	-55:2.5:55
Disturbance	Demand Power (kW)	Specified by driving cycle

The objective of the optimization problem is to maximize fuel economy while following the driving demand and to keep the SOC within reasonable range. The cost function is chosen as

$$J = \sum_{k=0}^{N-1} (fuel_k + \alpha \Delta_{SOC}^{\ 2}) \qquad \Delta_{SOC} = \begin{cases} SOC_k - SOC_d & SOC_k < SOC_d \\ 0 & SOC_k >= SOC_d \end{cases} \tag{14}$$

where the fuel consumed at each step $fuel_k$ is to be minimized and battery SOC_k is penalized when it is below the desired value SOC_d, with a positive weighting factor α. The optimization is subject to saturation constraints

$$\begin{aligned} &\omega_{e\_\min} \le \omega_{e\_k} \le \omega_{e\_\max} \\ &\omega_{m/g1\_\min} \le \omega_{m/g1\_k} \le \omega_{m/g1\_\max} \\ &T_{m/g1\_\min} \le T_{m/g1\_k} \le T_{m/g1\_\max} \\ &SOC_{\min} \le SOC_k \le SOC_{\max} \\ &P_{batt\_\min} \le P_{m/g1} + P_{m/g2} \le P_{batt\_\max} \end{aligned} \tag{15}$$

These inequality constraints are implemented by assigning large cost penalty to control decisions that lead to states or input signals that violate these saturation bounds.

Several techniques are applied when calculating the state transition tables, to reduce the computation requirement. Firstly, the speed constraint can be often examined before running the simulation. The speed of the M/G 1 can be determined and checked directly with specified ring gear speed and engine speed. For the cases with a M/G 1 speed which violates the constraint, it can be penalized immediately and hence eliminates the need to conduct the simulation all together. Secondly, instead of loading the simulation once and run one single case with specified states and inputs, Matlab allows us to load the simulation once and run a group of cases together. This is achieved by vectorizing the states and inputs. For instance, if the simulation is loaded with a SOC vector [0.4:0.003:0.7], and an engine throttle vector [0:0.025:1], and single specified value of the other states and inputs, it actually takes in a

matrix of cases, where each element presents one simulation case. The simulation can be made to run all the simulation cases together. Table II shows the comparison of computation time requirement between the two methods. It can be seen that computation time is reduced by a factor of 300. Thirdly, running Simulink in Matlab is slower compared with running the same simulation in a m-file. Therefore, all the simulations for calculating transition table are made in an m-file. This reduces the computation time by a factor of 10. With the help of all these techniques, a transition table computation which took days was found to finish in about three hours for an EPA driving cycle.

TABLE II
SIMULATION TIME (ORIGINAL SIMULATION VS VECTORIZATION APPOACH)

Simulation Cases	Simulation Approach	Simulation Time (sec)
We = 2900 rpm SOC = [0.4:0.003:0.7] Wr = 1195 rpm Throttle = [0:0.025:1] Tg = 0 Nm Pd = 7.4 kW	Simulate all cases one by one	153.6
	Simulate all cases at once	0.5

The developed DP program was used to produce vehicle behavior that shows what a global optimal solution looks like and serve as a benchmark for improving other control algorithms. Fig. 8 shows the power-split results of DP and the ECMS algorithm, during a typical vehicle speed cycle. This particular velocity profile is taken from the 5~45 second of the US06 driving cycle. A major difference of the power split behavior can be seen during vehicle acceleration (highlighted part). It seems that the DP algorithm uses battery power more than the ECMS algorithm if the battery SOC is high enough. This behavior was found to be universal rather than a special case for almost all of the accelerating maneuvers. We decide to focus on this particular behavior to seek opportunity to improve the ECMS algorithm.

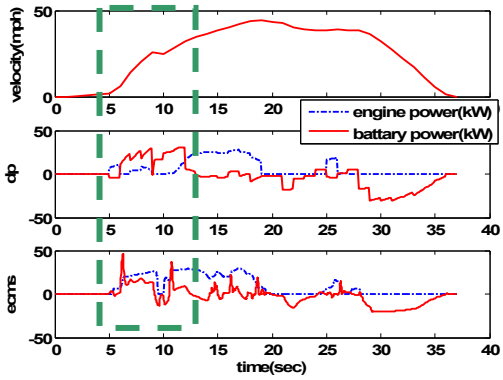

Fig. 8. Power split behavior of DP and ECMS control [US06].

In the ECMS algorithm as shown in (10)-(11), the speed constraints (15) is not taken into account. When the engine power demand is high, the engine optimal speed (for optimal engine efficiency) typically will also be high. If the vehicle speed happens to be low (such as the case when the vehicle is launching from a stand-still), M/G 1 must be pushed to a very high speed. This may result in M/G 1 speed saturation, which in turn results in the reduction of engine speed from the optimal speed. For example, in the case of THS system, if the engine power demand is 20 *kW*, then the engine needs to be running at ω_{e_d} =2333 *rpm* to achieve optimal efficiency. In this case, as shown in Fig. 9, due to the maximum M/G 1 speed constraint of 6500 *rpm*, the vehicle speed must be higher than 12.6 *mph*. Else, the M/G 1 speed constraint prevents the engine speed from operating at 2333 *rpm*. At higher engine power demand, the constraint is even more severe.

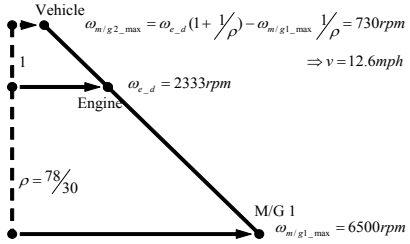

Fig. 9. Speed constraint calculation for THS.

V. IMPROVED ECMS CONTROL

An improved ECMS control is to be developed based on the discussions of the previous section. The speed constraint can be used as another factor to weight the battery equivalent consumption. Equation (10) is changed to

$$\dot{m}_{f\_equi}(t) = \dot{m}_{f\_eng} + g(v, F_d) f(soc) \cdot \dot{m}_{f\_batt}$$
$$g(P_d, v) = \begin{cases} 1 & P_d \le P(v) \\ 0.6 & P_d > P(v) \quad v \le v_c \end{cases} \qquad (16)$$

where v_c is the vehicle speed constraint calculated from the engine demand speed and the M/G 1 constraint speed. *P(v)* is the power required to maintain the vehicle at speed v. If the power demand is higher, the vehicle is accelerating. A coefficient $g(v,F_d)$ is then defined to change the weight of battery fuel equivalent consumption by considering the vehicle speed and power demand. Whenever the speed is lower and the vehicle is accelerating, we will use more battery power if the SOC is high enough.

Fig 10 shows the comparison results between the original control and the improved ECMS control algorithm. With the additional weighting factor, the battery picks up more power during launching, when power demand is high and vehicle speed is low. The additional weight prompts the preference to use battery power. The engine power demands reduces, which results in a reduction of desired engine speed. Therefore, M/G 1 does not need to be driven toward saturation. The generator torque demand during the transient also reduces, i.e. peak battery power is lower during the acceleration.

The fuel economy results of the simulated THS Prius vehicle under the EPA cycles are shown in Table III. The improved control strategy moves toward the optimal solution compare to the original ECMS design. This is

especially true for city cycles since there are more stop-go driving demands.

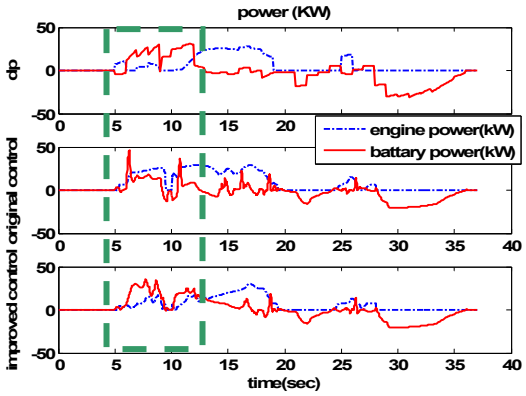

Fig. 10. Power split behavior of improved and original ECMS control [part of US06 cycle].

TABLE III
FUEL ECONOMY COMPARISON BETWEEN DIFFERENT CONTROLS ON THS

Fuel Consumption (mpg)	ECMS Control	Improved ECMS Control	DP
City	62	64	67
Highway	55	55	56

VI. CONCLUSION

A dynamic model of the Toyota Prius hybrid system was developed in this paper. As the first step, a controller based on the Equivalent Consumption Minimization Strategy (ECMS) was designed and implemented. This algorithm results in a perceived optimal power split between engine and battery power. The "speeder-torquer" concept is then used to control the operation of the "Motor" (M/G 2) and the "Generator" (M/G 1). The Dynamic Programming (DP) concept was utilized to obtain a benchmark behavior. After observing the DP behavior, modification to the ECMS algorithm was suggested, which achieves improved fuel economy.

ACKNOWLEDGEMENTS

This work is partially supported by Automotive Research Center of the University of Michigan, a Center of Excellence sponsored by the U.S. Army TARDEC under the contract DAAE07-98-C-R-L008.

REFERENCES

[1] Lin, C. C., Peng, H., Grizzle, J. W., Liu, J., and Busdiecker, M., "Control System Development for an Advanced-Technology Medium-Duty Hybrid Electric Truck", SAE Paper 2003-01-3369.

[2] Jalil, N., Kheir, N. A., and Salman, M., "A Rule-Based Energy Management Strategy for a Series Hybrid Vehicle", Proceedings of the American Control Conference, Albuquerque, New Mexico, Jun. 1997.

[3] Gelb, G. H., Richardson, N.A., Wang, T. C., Berman, B., "An Electromechanical Transmission for Hybrid Vehicle Power Trains – Design and Dynamometer Testing", *Society of Automotive Engineers*, paper No. 710235, SAE Congress, Detroit, MI. January 11-15, 1971.

[4] Miller, J. M. and Everett, M. "An assessment of ultra-capacitors as the power cache in Toyota THS-II, GM-Allision AHS-2 and Ford FHS hybrid propulsion systems", *Applied Power Electronics Conference and Exposition*, 2005. APEC 2005. Twentieth Annual IEEE, Page(s):481 - 490 Vol. 1.

[5] Sasaki, S., "Toyota's Newly Developed Hybrid Powertrain", Proceedings of the 1998 IEEE 10th International Symposium on Power Semiconductor Devices & IC's, Kyoto, Japan, 3-6 June, 1998.

[6] Harada, O., Yamaguchi, K., Shibata, Y., "Power output apparatus and method of controlling the same" *U.S. Patent* Number 6,067,801, issued May. 30, 2000.

[7] Hermance, D., "Toyota Hybrid System", *1999 SAE TOPTEC Conference*, Albany, NY, May 1999.

[8] Kimura, A., Abe, T., Sasaki, S., "Drive force control of a parallel-series hybrid system", *JSAE Review* Vol. 20, pp. 337-341, 1999.

[9] Duoba, M., Ng, H., and Larsen, R., "In-Situ Mapping and Analysis of the Toyota Prius HEV Engine", *SAE Paper* Number 2000-01-3096.

[10] Rousseau, A., Sharer, P., and Pasquier, M., "Validation Process of a HEV System Analysis Model: PSAT", *SAE Paper* Number 2001-01-0953.

[11] National Renewable Energy Laboratory, "Advanced Vehicle Simulator", http://www.ctts.nrel.gov/analysis/advisor.html, 2005.

[12] Duoba, M., Ng, H., and Larsen, R., "Characterization and Comparison of Two Hybrid Electric Vehicles (HEVs) – Honda Insight and Toyota Prius", *SAE Paper* Number 2001-01-1335.

[13] Muta, K., Yamazaki, M., and Tokieda, J. "Development of New-Generation Hybrid System THS II – Drastic Improvement of Power Perfomance and Fuel Economy", *SAE Paper* Number 2004-01-0064.

[14] Kawahashi, A., "A New-Generation Hybrid Electric Vehicle and Its Implications on Power Electronics," *CPES2004, Power Electronics Seminar & Industry Review*, VPI, Blacksburg, VA, 18-20 April 2004.

[15] Kimura, A., Ando, I., Itagaki, K., "Development of Hybrid System for SUV", *SAE Paper* Number 2005-01-0273.

[16] Zhang, H., Zhu, Y., Tian, G., Chen, Q., and Chen, Y., "Optimal Energy Management Strategy for Hybrid Electric Vehicles", *SAE Paper* Number 2004-01-0576.

[17] Rizoulis, D., Burl, J., and Beard, J., "Control Strategies for a Series-Parallel Hybrid Electric Vehicle", *SAE Paper* Number 2001-01-1354.

[18] Paganelli, G., Guezennec, Y., Rizzoni, G., "Optimizing Control Strategy for Hybrid Fuel Cell Vehicle", SAE 2002-01-0102.

[19] Bellman, R.E., *Dynamic Programming*, Princeton University Press, New Jersey, 1957.

[20] Benford, H., Leising, M., "The lever analogy: a new tool in transmission analysis", SAE Paper 810102.

[21] Liu, J., Peng, H., Filipi, Z., "Modeling and Control Analysis of Toyota Hybrid System", International Conference on Advanced Intelligent Mechatronics, Monterey, CA. Jul. 24-28, 2005.